NANO LETTERS

2003
Vol. 3, No. 8
1135−1139

Bone-Shaped Nanomaterials for Nanocomposite Applications

Terry T. Xu, Frank T. Fisher, L. Cate Brinson, and Rodney S. Ruoff*

Department of Mechanical Engineering, Northwestern University, Evanston, Illinois 60208

Received May 23, 2003; Revised Manuscript Received June 19, 2003

ABSTRACT

A novel template synthesis of bone-shaped (dumbbell-shaped, dogbone-shaped) nanomaterials is demonstrated. Porous anodic alumina (PAA) templates with uniform nanochannels were fabricated using a four-step anodization process and used to form bone-shaped carbon nanostructures with stem and end diameters and lengths of 40 nm, 70 nm, and 5 μm, respectively. These nanomaterials, which we refer to as bone-shaped T-CNTs (templated carbon nanotubes), have potential application in nanocomposites, where improved strength and toughness through mechanical interlocking is anticipated.

Nanocomposites, where nanoscale inclusions are embedded within a matrix material, have attracted increasing research attention in recent years. Reviews of such composites using nanoclays,[1−4] nanotubes,[5−7] and other nanostructures[8,9] are available in the literature. Here we will limit our focus to carbon nanotube−polymer composite systems, where researchers have found that the addition of small amounts of carbon nanotubes can appreciably enhance the mechanical properties of the nanocomposite compared to those of the unreinforced polymer. For example, the tensile strength of polystyrene was increased 25% by adding only 1 wt % of multiwalled carbon nanotubes (MWCNTs).[10] Although promising, the mechanical properties obtained in these initial experiments have not achieved those values predicted by theoretical calculations or atomistic simulations.[11−14]

The effective development of nanotube-reinforced polymers is contingent on the ability to disperse the nanotubes uniformly within the polymer and the effectiveness of nanotube−polymer load-transfer mechanisms.[15] Specifically, nanotube−polymer load transfer will play an important role in the optimization of the mechanical properties of these materials. One method of enhancing the load transfer in these systems is to strengthen the chemical interactions at the interface. Considerable efforts to functionalize carbon nanotubes to enhance these effects are ongoing.[16−18] Another means to improve the load-transfer characteristics of the material is to facilitate nanoscale mechanical interlocking between the nanotubes and polymer. For one particular nanotube−polymer system, researchers have found that a key factor in load transfer across the interface is the helical conformation of the polymer around the NT. This molecular-level entanglement was found to dominate binding energy and frictional force effects in determining the efficiency of load transfer between the polymer and the nanotubes.[19] In this paper, we demonstrate the fabrication of bone-shaped carbon nanostructures. On the basis of experimental results for composites with macro-sized bone-shaped fibers, these nanostructures are projected to enhance nanoscale mechanical interlocking load-transfer mechanisms.

The concept of bone-shaped short (BSS) fiber composites[20] has been the subject of a recent review article.[21] The approach involves creating short fibers having a constant-diameter intermediate (stem) section and enlarged ends. Several model composite systems with macro-sized inclusions have been studied, including BSS nickel fiber-reinforced polymer matrix composites, BSS polyethylene fiber-reinforced polyester matrix composites, and BSS steel wire-reinforced concrete.[21] Experimental results on these systems suggest that an optimized bone-shaped morphology has the potential to improve both the strength and toughness of composite systems significantly.[21−23] For short-fiber composites, strength and toughness typically have an inverse relationship; strong interfaces that promote high load transfer (and hence strength) cannot relieve stresses in front of an approaching crack and thus have low fracture toughness. However, whereas systems with a weak interface have higher fracture toughness characteristics due to the energy-dissipating mechanisms of fiber−matrix sliding, they typically have reduced strength due to the ease of fiber pull-out from the matrix.

The advantage of the bone-shaped morphology for short-fiber composites is that the enlarged fiber ends allow load to be effectively transferred from the matrix to the reinforcing fiber (promoting high strength) without relying on an overly strong fiber−matrix interface. Motivated by these results with

* To whom all correspondence should be addressed. E-mail: r-ruoff@northwestern.edu. Tel: (847) 467-6596. Fax: (847) 491-3915.

10.1021/nl0343396 CCC: $25.00
Published on Web 07/16/2003

macro-sized bone-shaped fibers, we sought to synthesize bone-shaped nanostructures for nanocomposite applications. Analogous to the macro-sized BSS samples[21,22] described above, we believe that bone-shaped nanostructures will provide an additional load-transfer mechanism via mechanical interlocking of the enlarged ends within the matrix. This will likely result in additional mechanical property enhancement for nanocomposites. The unique geometry of these nanostructures is also likely to be advantageous for other applications, such as field-effect transistors.[24]

In this letter, we demonstrate a general utility synthesis procedure for the templated fabrication of bone-shaped nanomaterials. Specifically, we have developed a novel procedure for the creation of porous anodic alumina (PAA) films[25,26] using a modified four-step anodization process. Although other multistep anodization processes have been presented in the literature,[24] our modified four-step process produces PAA films with a close-packed array of uniform bone-shaped nanochannels (coexisting with funnel-shaped nanochannels as discussed below). These PAA films are then available as a template for the deposition of a suitable precursor. To demonstrate this procedure, bone-shaped carbon nanostructures were synthesized via pyrolysis of ethylene inside the PAA film. The as-synthesized bone-shaped carbon nanomaterials have a stem diameter of ~40 nm, a diameter at the two widened ends of ~70 nm, and an overall length of ~5 μm. As discussed below, the bone-shaped nanostructure geometry can be varied by appropriately selecting the PAA film fabrication parameters and precursor deposition conditions.

The fabrication procedure for a PAA film having bone-shaped nanochannels is schematically shown in Figure 1. High-purity aluminum foil (Alfa Aesar, 0.5 mm thick, Puratronic, 99.998%) was subjected to a four-step anodization. The first anodization was carried out at a constant voltage of 40 V in 0.3 M oxalic acid at 10 °C for 5 h (a). The resulting thin alumina film was then stripped off in a mixture of phosphoric acid and chromic acid (47.2 mL of CrO_3 + 7 mL of H_3PO_4 + 145.8 mL of H_2O) at 85 °C for 40 min (b). This strip-off process exposed well-ordered concave patterns on the aluminum substrate that act as self-assembled masks for the second anodization process.[25,26] The second anodization was performed for 5 min under the same conditions as in the first anodization step, creating partial nanochannels having a diameter of ~40 nm and a depth of ~350 nm (c). The interpore distance here is approximately 100 nm. These nanochannels were then widened in 0.1 M H_3PO_4 at 40 °C for 25 min (d), which increases the nanochannel diameters to ~70 nm. After this pore-widening step, the third anodization was carried out for 40 min under the same conditions as in the first anodization step to create funnel-like nanochannels (e). The fourth anodization was carried out at a higher voltage (80 V) in 0.04 M oxalic acid at 17 °C for 3 min to widen the opposite ends of the nanochannels (f). Nail polish (Sally Hansen Maximum Growth) was then coated on the top surface of the PAA film (g), which serves as a protective layer for the subsequent etching of the aluminum substrate in a $CuCl_2$-based solution at 10 °C for roughly 30 min (h).[27] Removal of the nail polish layer using acetone (i) leaves a clean PAA film for the subsequent carbon deposition process.

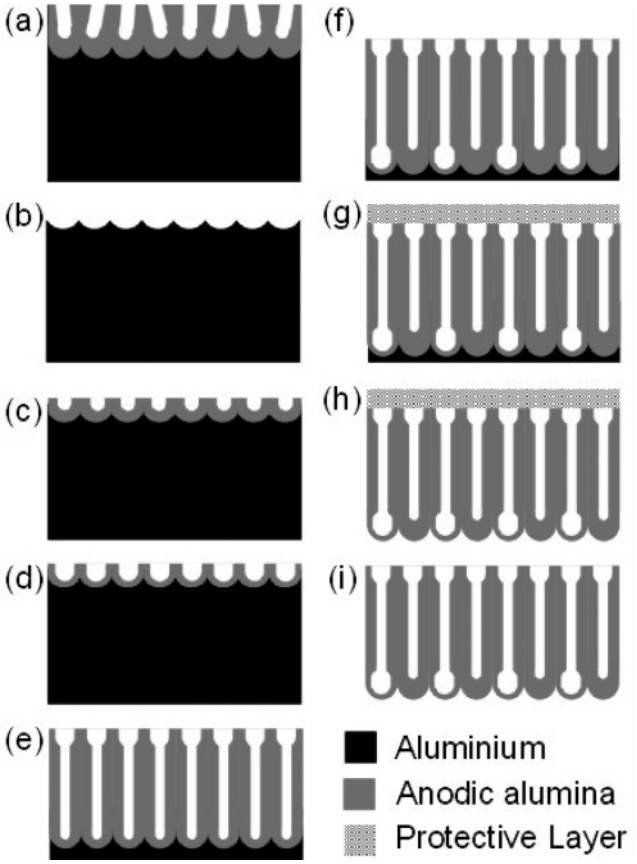

Figure 1. Schematic drawing of the fabrication procedure for a PAA film having bone-shaped nanochannels. (a) Formation of the porous alumina layer after the first anodization. (b) Removal of the porous anodic alumina layer. (c) Formation of the ordered porous alumina layer after the second anodization. (d) Chemical etching to widen the nanochannels. (e) Third anodization creates funnel-like nanochannels. (f) Fourth anodization at higher anodization voltage to widen the opposite ends of the nanochannels. (g) Protective-layer coating. (h) Removal of the aluminum layer. (i) Removal of the protective layer.

The as-fabricated PAA film was cut into several pieces using a razor blade for characterization in a scanning electron microscope (SEM; LEO 1525). Figure 2 shows SEM micrographs of the cross section of the PAA film. Figure 2a shows that the film is composed of three portions (i.e., End1, End2, and the intermediate stem). As illustrated in Figure 1, End1 and End2 were widened by different methods. End1 was widened by chemical etching, whereas End2 was widened by an increase in the anodization voltage. Figure 2b is the enlarged view of End1, showing that each nanochannel was widened after chemical etching. The funnel-like shape of the pore is clearly visible in the image. Figure 2c is the enlarged view of End2, showing that only a few nanochannels were widened and continued to grow during the fourth anodization step as indicated by the arrows. It is well known that during the anodization process the pore diameter (D) and interpore distance (d_{int}) in the anodic alumina are each directly proportional to the anodization

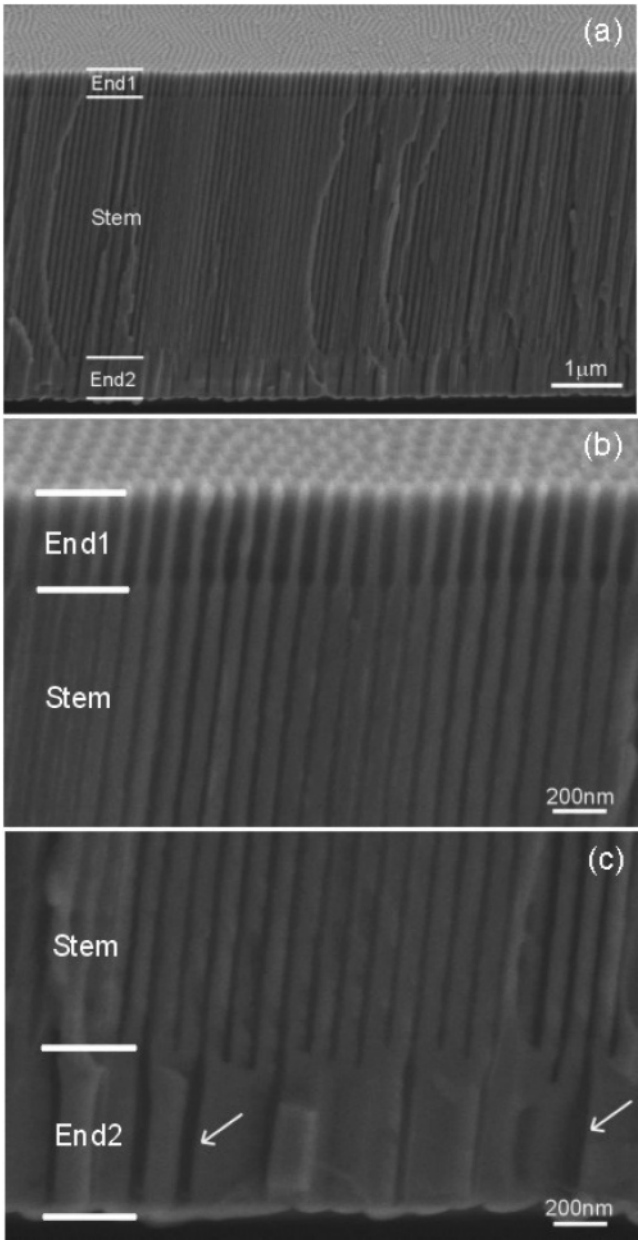

Figure 2. SEM micrographs of the bone-shaped PAA film cross section. (a) Overall image of the PAA film showing three nanochannel regions: End1, the intermediate stem, and End2. (b) High-magnification image of End1, showing that each nanochannel (appearing dark in the image) was widened by chemical etching. The funnel-like shape of the pore can be clearly identified. (c) Higher-magnification image of End2 grown at double the original anodization voltage, showing that only select nanochannels continued to grow at the wider diameter. The arrows in this image indicate the pores that have been widened during the fourth anodization step.

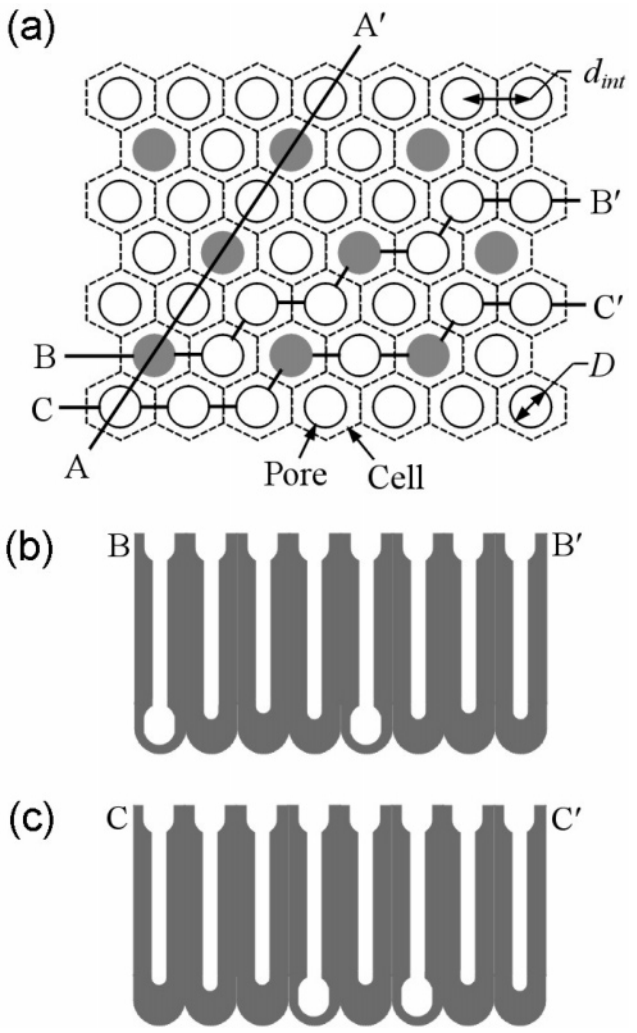

Figure 3. (a) Schematic drawing of cell/pore arrangement in the PAA film. White circles represent the original pores formed during the first anodization. Gray circles represent the positions where the original pores can continue to grow and be widened if the anodization voltage is doubled. Lines AA′, BB′, and CC′ indicate three possible cleavage planes when fracturing the PAA film. (b) Cross section of the cleavage plane along BB′. (c) Cross section of the cleavage plane along CC′. The cross-section of the cleavage plane for AA′ is illustrated in Figure 1i.

voltage.[28] Therefore, an increase or decrease in the anodization voltage leads to a redistribution of pore and cell populations. For example, increasing the anodization voltage will result in the termination of the growth of certain pores so that the remaining pores can continue to grow at a larger diameter. Decreasing the anodization voltage will cause the initiation of smaller pores, resulting in the formation of branched nanochannels.[28]

The ideal geometry of anodic alumina can be represented as a honeycomb structure, which is characterized by a close-packed array of columnar hexagonal cells, each containing a central pore normal to the substrate.[25,26,28] The dimensions of the PAA films are tunable, to a certain extent, by the film fabrication parameters. For example, the cell/pore size is determined by several factors, such as the anodization voltage and electrolyte type. The thickness of the PAA film is controlled by the anodization time.[28] Figure 3a is a schematic of the top view of the pore/cell arrangement. As discussed previously, because the interpore spacing d_{int} is proportional to the anodization voltage V (i.e., $d_{int} = k$ V, where $k \approx 2.5-2.8$ nm/V),[29,30] an integer multiple increase in the anodization voltage will result in the new d_{int} being an integer multiple of the original interpore distance. Thus, the resultant pore arrangement will still be ordered. As an example, the gray regions in Figure 3a represent positions where the pores

will be widened and continued to grow if the voltage is doubled during the anodization. On the basis of this configuration, it can be estimated that the yield ratio of bone-shaped to funnel-shaped nanochannels is 1:3. Also shown in Figure 3a are three possible cleavage planes that can be produced upon fracture of the PAA film. Clearly, the cross-sectional view of the PAA film will vary with the cleavage plane. If the fracture occurs along AA′, then the cross-sectional view will be that shown in Figure 1i. If the fracture occurs along other paths (e.g., BB′ or CC′), then a different morphology will be observed (Figure 3b and c).

For the formation of bone-shaped carbon nanostructures, the PAA film was placed in a tube furnace (Lindberg), heated to 700 °C, and kept for 1 h in the presence of flowing ethylene (Air Products CP min. purity 99.8%; 20 sccm) and argon (Air Products research grade, purity 99.995%; 20 sccm). The thermal decomposition of the precursor ethylene gas in the nanochannels of the PAA film results in carbon deposition on the channel walls.[31,32] Depending on the deposition time and conditions, tubelike or rodlike nanostructures can be synthesized.[31,32] After the deposition was completed, the PAA film was dissolved using 6 M NaOH at 40 °C for 24 h, leaving the free-standing, bone-shaped carbon nanostructures. Although here we demonstrate templated carbon bone-shaped nanostructures, we note that this technique can be adapted to create a wide range (e.g., Ni, Ag, metal oxide, etc.) of bone-shaped nanostructures.[33−35]

These carbon nanostructures were then characterized by transmission electron microscopy (TEM; Hitachi HF2000, H8100). Figure 4a shows a TEM image of a bundle of bone-shaped and funnel-shaped carbon nanostructures. End1 and End2 can be easily distinguished from the stem in the image. Figure 4b shows an individual bone-shaped carbon nanostructure. From the image, we conclude that it is hollow. Although not identical to the BSS macroscale fibers (which typically have more "stubby" ends[21]), we suggest the nomenclature "bone-shaped T-CNTs" (templated carbon nanotubes). The ensemble of fabricated bone-shaped T-CNTs are quite uniform, with lengths (L) of ∼5 μm and diameters of ∼40 and ∼70 nm, respectively, for the intermediate stem (D_{stem}) and widened end regions (D_{ends}). Figure 4c shows a close view of the joint portion between the stem and the widened end. The wall thickness is approximately 10 nm. A representative lattice image of the as-synthesized T-CNTs is shown in Figure 4d. Rather than perfect graphitic layers, disordered carbon layers are observed, indicating that the T-CNTs have a turbostratic (not fully graphitized) structure.[36] The inset in Figure 4d is the selected area diffraction (SAD) pattern. The 002 diffraction has the appearance of a pair of small arcs (indicated by white arrows in the inset), confirming the low crystallinity of these bone-shaped T-CNTs. The fraction of sp^2-bonded atoms estimated from the electron energy-loss spectroscopy (EELS) spectrum is approximately 0.7,[37] which again confirms that the as-synthesized carbon nanostructures are not fully graphitized. It is not surprising that these T-CNTs have low crystallinity, as no catalyst was used during their synthesis. Post-synthesis graphitization of

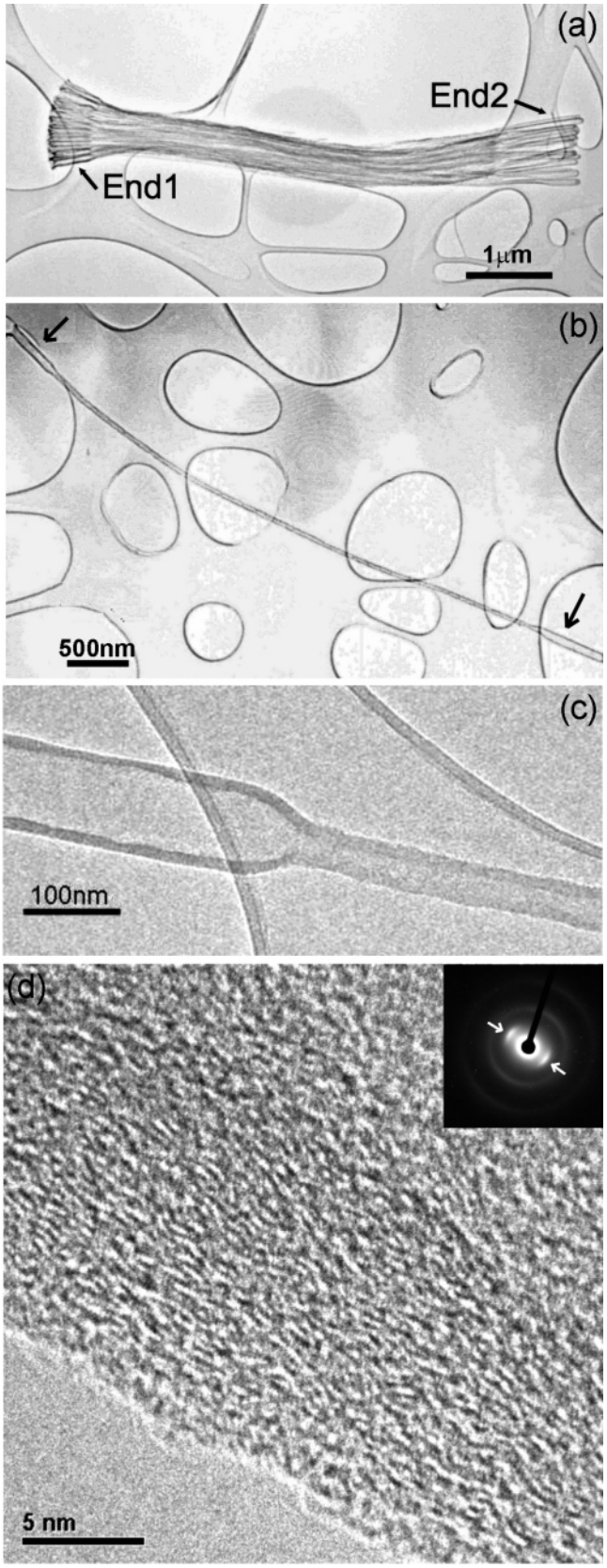

Figure 4. (a) TEM image of a bundle of bone-shaped and funnel-shaped T-CNTs. (b) TEM image of an individual bone-shaped T-CNT. (c) TEM image of the joint portion between the stem and the widened end. (d) Lattice image of an as-synthsized bone-shaped T-CNT showing a turbostratic structure. (The inset is the corresponding SAD pattern.)

these T-CNTs at 2800 °C may improve their mechanical properties.[31,32]

By varying the anodization and deposition parameters, it is possible to a certain extent to fabricate T-CNTs of tunable dimensions. For example, using a combination of sulfuric acid and oxalic acid, we have separately fabricated nanochannel templates having stem and end diameters of ∼20 and ∼40 nm, respectively. The length of the nanochannels is governed by the anodization time, and the wall thickness of the T-CNTs is controlled by the precursor deposition time. However, we note that there are some limitations to the bone-shaped geometries that can be made using the current technique. Because $d_{int}/D \approx 3$,[29] the maximum diameter of the widened ends cannot exceed 3 times that of the stem. Finally, to maximize the mechanical property enhancement of the T-CNT-reinforced nanocomposites, the geometry (D_{stem}/D_{ends}, L) of the bone-shaped nanostructures should be optimized using the results of numerical modeling and experimental studies. We have initiated fundamental studies of these bone-shaped nanostructures as reinforcement in polymer matrix composites to determine the optimal bone-shaped structure for composite strength and toughness. Whereas the aspect ratio (L/D_{stem}) of the samples described here is 125, control of the pore diameter and thickness of the PAA template gives great flexibility in the aspect ratios achievable using this technique.

In conclusion, we have presented a novel approach for the template synthesis of bone-shaped nanomaterials. A procedure for creating a PAA film having bone-shaped nanochannels was developed, and this template was used to form bone-shaped carbon nanotubes from an ethylene gas precursor. The geometry of the nanochannels is tunable by using different anodization parameters. The bone-shaped templated carbon nanotubes (bone-shaped T-CNT) described here have a stem diameter of ∼40 nm, enlarged end diameters of ∼70 nm, and a length of ∼5 μm. The crystalline structure of these bone-shaped T-CNTs appeared to be turbostratic. We are currently extending this template synthesis method to create other bone-shaped nanostructured materials, as well as investigating the use and optimization of these bone-shaped nanostructures in composites applications.

Acknowledgment. R.S.R. gratefully acknowledges support from the Office of Naval Research Mechanics of Nanostructures under grant award no. N000140210870. R.S.R. and L.C.B. also appreciate support from the NASA University Research, Engineering and Technology Institute on Bio Inspired Materials (BIMat) under award no. NCC-1-02037 and from the NASA Langley Research Center Computational Materials: Nanotechnology Modeling and Simulation Program.

Note Added after ASAP: The ratio of bone-shaped to funnel-shaped nanochannels (1:2) has been corrected to 1:3. This paper was originally published ASAP on 7/16/2003. The corrected version was reposted on 7/18/2003.

References

(1) Biswas, M.; Ray, S. S. In *New Polymerization Techniques and Synthetic Methodologies*; Springer-Verlag: Berlin, 2001; Vol. 155, p 167.
(2) LeBaron, P. C.; Wang, Z.; Pinnavaia, T. J. *Appl. Clay Sci.* **1999**, *15*, 11.
(3) Alexandre, M.; Dubois, P. *Mater. Sci. Eng., R* **2000**, *28*, 1.
(4) Schmidt, D.; Shah, D.; Giannelis, E. P. *Curr. Opin. Solid State Mater. Sci.* **2002**, *6*, 205.
(5) Thostenson, E. T.; Ren, Z. F.; Chou, T. W. *Compos. Sci. Technol.* **2001**, *61*, 1899.
(6) Qian, D.; Wagner, G. J.; Liu, W. K.; Yu, M.-F.; Ruoff, R. S. *Appl. Mech. Rev.* **2002**, *55*, 495.
(7) Lau, K. T.; Hui, D. *Composites, Part B* **2002**, *33*, 263.
(8) *Polymer Nanocomposites: Synthesis, Characterization, and Modeling*; Krishnamoorti, R., Vaia, R. A., Eds.; ACS Symposium Series 804; American Chemical Society: Washington, DC, 2001.
(9) Li, J. Y. In *Handbook of Nanophase and Nanostructured Materials*; Wang, Z. L., Liu, Y., Zhang, Z., Eds.; Materials Systems and Applications; Kluwer Academic/Plenum Publishers: New York, 2003; Vol. 4, p 69.
(10) Qian, D.; Dickey, E. C.; Andrews, R.; Rantell, T. *Appl. Phys. Lett.* **2000**, *76*, 2868.
(11) Fisher, F. T.; Bradshaw, R. D.; Brinson, L. C. *Appl. Phys. Lett.* **2002**, *80*, 4647.
(12) Fisher, F. T.; Bradshaw, R. D.; Brinson, L. C. *Compos. Sci. Technol.* **2003**, *63*, 1689.
(13) Bradshaw, R. D.; Fisher, F. T.; Brinson, L. C. *Compos. Sci. Technol.* **2003**, *63*, 1705.
(14) Liao, K.; Li, S. *Appl. Phys. Lett.* **2001**, *79*, 4225.
(15) Schadler, L. S.; Giannaris, S. C.; Ajayan, P. M. *Appl. Phys. Lett.* **1998**, *73*, 3842.
(16) Gong, X.; Liu, J.; Baskaran, S.; Voise, R. D.; Young, J. S. *Chem. Mater.* **2000**, *12*, 1049.
(17) Czerw, R.; Guo, Z. X.; Ajayan, P. M.; Sun, Y. P.; Carroll, D. L. *Nano Lett.* **2001**, *1*, 423.
(18) Sinnott, S. B. *J. Nanosci. Nanotechnol.* **2002**, *2*, 113.
(19) Lordi, V.; Yao, N. *J. Mater. Res.* **2000**, *15*, 2770.
(20) Zhou, B. *J. Mater. Sci. Technol.* **1993**, *9*, 9.
(21) Zhu, Y. T.; Beyerlein, I. J. *Mater. Sci. Eng., A* **2002**, *326*, 208.
(22) Wetherhold, R. C.; Lee, F. K. *Compos. Sci. Technol.* **2001**, *61*, 517.
(23) Zhu, Y. T.; Beyerlein, I. J.; Valdez, J. A.; Lowe, T. C. *Mater. Sci. Eng., A* **2001**, *317*, 93.
(24) Lee, J. S.; Gu, G. H.; Kim, H.; Jeong, K. S.; Bae, J.; Suh, J. S. *Chem. Mater.* **2001**, *13*, 2387.
(25) Masuda, H.; Fukuda, K. *Science* **1995**, *268*, 1466.
(26) Masuda, H.; Satoh, M. *Jpn. J. Appl. Phys., Part 2* **1996**, *35*, L126.
(27) Xu, T. T.; Piner, R. D.; Ruoff, R. S. *Langmuir* **2003**, *19*, 1443.
(28) O'Sullivan, J. P.; Wood, G. C. *Proc. R. Soc. London, Ser. A* **1970**, *317*, 511.
(29) Lira, H. D. L.; Paterson, R. *J. Membr. Sci.* **2002**, *206*, 375.
(30) Nielsch, K.; Choi, J.; Schwirn, K.; Wehrspohn, R. B.; Gosele, U. *Nano Lett.* **2002**, *2*, 677.
(31) Kyotani, T.; Tsai, L. F.; Tomita, A. *Chem. Mater.* **1996**, *8*, 2109.
(32) Kyotani, T.; Tomita, A. *Surf. Sci. Ser.* **2000**, *92*, 552.
(33) Nielsch, K.; Wehrspohn, R. B.; Barthel, J.; Kirschner, J.; Gosele, U.; Fischer, S. F.; Kronmuller, H. *Appl. Phys. Lett.* **2001**, *79*, 1360.
(34) Lakshmi, B. B.; Dorhout, P. K.; Martin, C. R. *Chem. Mater.* **1997**, *9*, 857.
(35) Zhang, J.; Wang, X.; Peng, X.; Zhang, L. *Appl. Phys. A* **2002**, *75*, 485.
(36) *Graphite Fibers and Filaments*; Dresselhaus, M. S., Dresselhaus, G., Sugihara, K., Spain, I. A., Goldberg, H. A., Eds.; Springer-Verlag: New York, 1988; p 9.
(37) Kulik, J.; Lifshitz, Y.; Lempert, G. D.; Rabalais, J. W.; Marton, D. *J. Appl. Phys.* **1994**, *76*, 5063.

NL0343396